



# Experimental demonstration of pressurized chemical looping combustion in an internally circulating reactor for power production with integrated CO<sub>2</sub> capture

Mogahid Osman<sup>a</sup>, Abdelghafour Zaabout<sup>b</sup>, Schalk Cloete<sup>b</sup>, Shahriar Amini<sup>a,b,\*</sup>

<sup>a</sup> Norwegian University of Science and Technology, Department of Energy and Process Engineering, Norway

<sup>b</sup> SINTEF Industry, Process Technology Department, Trondheim, Norway

## HIGHLIGHTS

- Internally circulating reactor (ICR) was demonstrated for chemical looping combustion at pressurized condition up to 6.0 bar.
- The ICR is proposed and design to simplify the operation and scale-up of chemical looping processes at high-pressure.
- The solids circulation rate was found to increase with increasing the operating pressure at a constant fluidization velocity.
- CO<sub>2</sub> capture efficiency and purity up to 97% was achieved, and found to be insensitive to the operating pressure.
- Autothermal high-pressure CLC operation using ICR was achieved.

## ARTICLE INFO

### Keywords:

Chemical looping combustion  
High pressure operation  
Internally circulating reactor  
Fluidized-bed, CO<sub>2</sub> capture  
Correlation for solids circulation rate

## ABSTRACT

This study presents an experimental demonstration of pressurized chemical looping combustion (CLC) in an internally circulating reactor (ICR). The ICR concept is a novel alternative to the conventional interconnected fluidized bed CLC configuration as it eliminates all cyclones, loop seals and solids transport lines, and it can be pressurized in a single pressure shell. Stable operation with high fuel conversion was established for about 40 h of operation at pressures up to 6 bar, achieving reasonable CO<sub>2</sub> purity and capture efficiency (up to 97%). The solids circulation rate was found to increase with increasing the operating pressure at a constant fluidization velocity with no effect on CO<sub>2</sub> capture and purity. The experimental campaign also examined the effects of solids inventory and fluidization velocities in the air and fuel reactors. The CO<sub>2</sub> purity and capture efficiency were most sensitive to the solids inventory, whereas the solids circulation rate was most sensitive to the air reactor fluidization velocity and the solids inventory. A correlation for solids circulation rate was derived from the collected experimental data, thus providing a robust tool for designing an ICR system for pressurized operation. This correlation can assist in further scale-up and demonstration of the ICR concept in commercial scale.

## 1. Introduction

Carbon capture and storage (CCS) has a great potential of reducing CO<sub>2</sub> emissions from the utilization of fossil fuels, which would play a significant role in fulfilling the ambitions of the Paris agreement to limit future temperature rise below 2 °C [1]. Various technologies for CCS have been introduced in the last decades with a reduction in the energy penalty of CO<sub>2</sub> capture as one of the main objectives. Chemical looping combustion (CLC) is a promising technology for power production based on fossil fuels combustion with integrated CO<sub>2</sub> capture and with a reduced energy penalty. The CLC system carried out in two steps, in the

fuel reactor the fuel interacts with an oxygen carrier (metal oxide) to fully oxidize to CO<sub>2</sub> and H<sub>2</sub>O, the reduced metal oxide is re-oxidized in a flow of air in the air reactor, ready to start a new cycle and producing heat for power production [2–4]. If the CLC system is pressurized, the hot depleted air from the air reactor can be used for efficient power generation in a downstream combined cycle.

Pressurized chemical looping combustion (PCLC) therefore has the potential for maximizing the power plant efficiency by using a combined cycle instead of the steam cycle used with atmospheric pressure boilers. In addition, high pressure combustion increases the condensate temperature, hence, the condensate in the fuel reactor outlet stream can

\* Corresponding author at SINTEF Industry, S.P. Andersens vei 15 B, 7031, Trondheim, Norway.

E-mail address: [shahriar.amini@sintef.no](mailto:shahriar.amini@sintef.no) (S. Amini).

<https://doi.org/10.1016/j.cej.2020.125974>

Received 19 March 2020; Received in revised form 22 May 2020; Accepted 17 June 2020

Available online 23 June 2020

1385-8947/ © 2020 The Authors. Published by Elsevier B.V. This is an open access article under the CC BY license (<http://creativecommons.org/licenses/by/4.0/>).

**Nomenclature**

AR	Air reactor
CLC	Chemical looping combustion
FR	Fuel reactor
ICR	Internally circulating reactor
OC	Oxygen carrier
$F_{iCO}$	CO molar flowrate at FR inlet (mol/min)
$F_{oCO}$	CO molar flowrate at FR outlet (mol/min)
$F_{AR,oCO_2}$	CO <sub>2</sub> flowrate at AR outlet (NI/min)
$F_{FR,iCO}$	CO flowrate at FR inlet (NI/min)
$F_{FR,oCO_2}$	CO <sub>2</sub> flowrate at FR outlet (NI/min)
$F_{FR,o_{tot}}$	Total FR outlet flowrate (NI/min)
$F_{FR,iN_2}$	N <sub>2</sub> flowrate at FR inlet (NI/min)

$F_{O_2,AR,in}$	Inlet molar flowrate of oxygen to the AR
$m_{OC}$	Actual mass of the OC in its partially oxidized state (g)
$m_{OC_{ox}}$	Mass of the fully oxidized OC (g)
$m_{O_2}$	Mass of O <sub>2</sub> consumed during the re-oxidation test (g)
$\dot{m}_s$	Solids circulation rate (g/s)
$M_{O_2}$	Molecular weight of oxygen
$\dot{n}_{CO}$	Molar flowrate of CO (mol/s)
$R_o$	Oxygen transport capacity of the OC
$X_{s,FR}$	Solids conversion in FR
$X_{s,AR}$	Solids conversion in AR
$X_{O_2}$	Oxygen conversion at outlet of AR
$\Delta X_s$	Solids conversion difference between AR and FR
$\gamma_{CO}$	Conversion of CO, %

be utilized as a heat source within the process, which increases the thermal energy recovery from the fuel (the higher heating value instead of the lower heating value). This is especially magnified for CLC with natural gas given the high moisture content in the fuel reactor flue gas. Other benefits for high pressure CLC operation include: reduced power consumption for CO<sub>2</sub> compression and/or refrigeration steps, and increased heat transfer rates. Thermodynamic investigations has revealed that the integration of PCLC with a natural gas fired combined cycle (NGCC) can achieve a power efficiency of 52 to 55% (LHV), that is higher than NGCC with post-combustion CO<sub>2</sub> capture by 3–5% points [5,6]. Pressurized CLC is also applicable to solid fuels using integrated gasification combined cycle (IGCC) power plant configurations. Compared to conventional pre-combustion CO<sub>2</sub> capture, such CLC-IGCC plants can also improve power plant efficiency by 3–5% points [7]. The challenge of relatively low turbine inlet temperatures limited by the maximum operating temperature of the CLC reactors can be mitigated by using an added combustor after the CLC reactors as has been simulated for NGCC [8,9] and IGCC power plants [10]. Such added firing can almost eliminate the CO<sub>2</sub> capture energy penalty, but it introduces additional costs when firing with hydrogen or additional emissions

when firing with natural gas.

The circulating fluidized-bed reactor (CFB) is the mostly used reactor configuration for chemical looping processes at a lab [2,11,12] and pilot scales [3,13]. The CFB system consists of two separate reactors connected with a loop seals and cyclones for gas–solid separation. Pressurized operation in such a highly interconnected system will impose several challenges. First, each reactor, cyclone, loop seal and solids transport line must be designed in a separate pressure shell to ensure mechanical integrity under pressurized operation at very high temperatures. Second, any pressure imbalance can lead to significant instabilities in the solids circulation rate, and may lower the performance of loop seals and cyclones causing a high gas leakage between the two reactors. Third, the required fluidization steam for the loop seals will increase with increasing pressure, which would result in a higher energy penalty [14]. These challenges prompted research on different reactor configurations with the potential ability to operate under pressurized conditions. These configurations include gas switching concept [15–17], moving bed [18,19], rotating bed reactor [20,21] and the internally circulating fluidized-bed reactor (ICR) [22,23], which will be the focus of the current study.

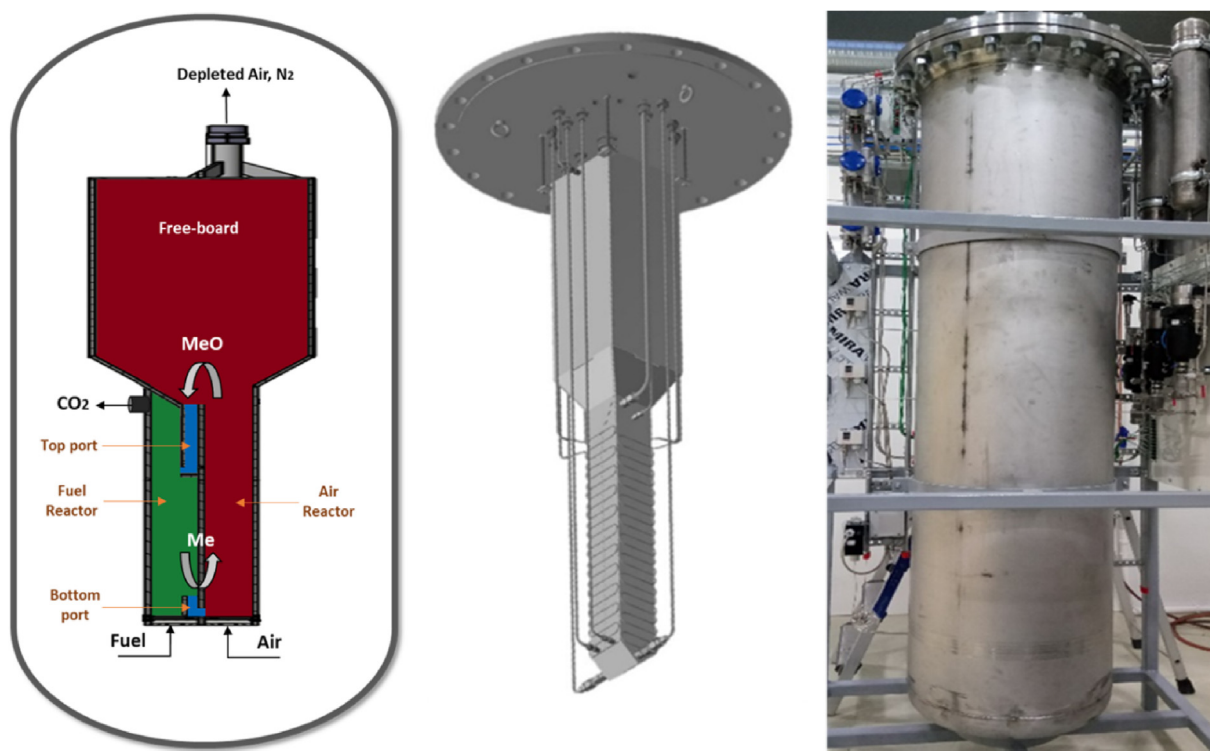


Fig. 1. From left to right; a simplified scheme of the ICR design, CAD drawing of the ICR unit, and the ICR unit under operation inside the shell.

The ICR incorporates many of the operational capabilities of the circulating fluidized-bed reactor, while eliminating the complex separation systems (i.e., cyclone and loop seals). Specifically, the ICR concept aims to simplify the design, ease the solids circulation, and operate at high pressure easily in a single pressurized vessel. The ICR concept (as shown in Fig. 1) is a single vessel unit with two chambers connected by ports (one in the top and the second at the bottom), and a freeboard. The two ports replace the loop seals involved in the CFB, while the freeboard replaces the cyclones making the ICR reactor design compact while maintaining the same benefits and functionalities of the CFB reactors. The oxygen carrier circulation in ICR attained through feeding higher gaseous velocity in the air reactor (AR) than in the fuel reactor (FR). The solids transported to the freeboard decelerate and falls to the FR through the top port. The accumulation of solids in FR led to static pressure build-up that forces the solids to circulate back to the AR through the bottom port. This simple solids circulation mechanism combined with the compact design make the ICR concept very suitable for pressurized operation. The use of a freeboard instead of cyclones for gas solid separation after the air reactor will also reduce particle elutriation.

The major trade-off of the simplicity obtained by the ICR concept is the gas leakage between the two reactor sections through the connecting ports, reducing CO<sub>2</sub> capture efficiency and purity. Large gas leakages could also raise safety concerns from direct contact of air and fuel. This is of lower concern in the lower port because any large heat release would be quickly absorbed by the high heat capacity of the particles. No particles are present to control a large heat release at the top port, but as long as complete fuel conversion is achieved in the fuel reactor, there is no risk. However, the demonstration of the current ICR for atmospheric CLC operation showed that the gas leakage can be easily minimized by controlling the fluidization velocity ratio of the two chambers and the solids inventory, attaining CO<sub>2</sub> capture efficiency and purity greater than 95% [24]. The current ICR unit had also been used for chemical looping reforming of methane at atmospheric operation [23]. The reactor showed promising performance in terms of gas leakage, solids circulation rate, fuel conversion and revealed a simple

approach to control its performance over a wide range of operating conditions.

Following the successful operation of ICR under atmospheric operation, the current study aimed to experimentally investigate the ICR behavior for gaseous fuel CLC under pressurized operation. The largest focus of this study falls on re-evaluating the effect of process parameters such as solids loading and gas fluidization velocity under pressurized conditions on the ICR performance indicators such as gas leakage between the chambers, fuel conversion and solids circulation rate. Given the importance of the latter in accurate design of large-scale pressurized ICR reactors, a correlation linking the solids circulation rate to the process parameters was extracted experimentally at an operating pressure range of 1 to 6 bar. NiO-based oxygen carrier and CO as a fuel were used for the chemical looping combustion experiments. This study represents the first demonstration of the ICR concept under pressurized conditions for CLC.

## 2. Methodology

### 2.1. ICR unit

The ICR unit is a single reactor vessel that consists of two separate chambers; AR and FR (air and fuel reactors), connected through two ports at the top and the bottom and a freeboard (Fig. 1). The unit is enclosed in a cylindrical shell to enable operation at high pressure. The two connecting ports were designed to facilitate solids circulation between the two chambers while minimizing gas leakage and the freeboard aimed to decelerate the solids and minimize particle elutriation in the AR. Further details about the ICR unit design and specifications can be found in previous studies, in which this ICR unit was demonstrated for chemical looping combustion and reforming under atmospheric conditions [23,24].

Fig. 2 illustrates the layout of the various auxiliary components of the ICR unit beside the main reactor vessel. A water heat exchanger used for cooling down the exhaust gaseous from the AR and the FR before being vented to the atmosphere, followed by particle filters to

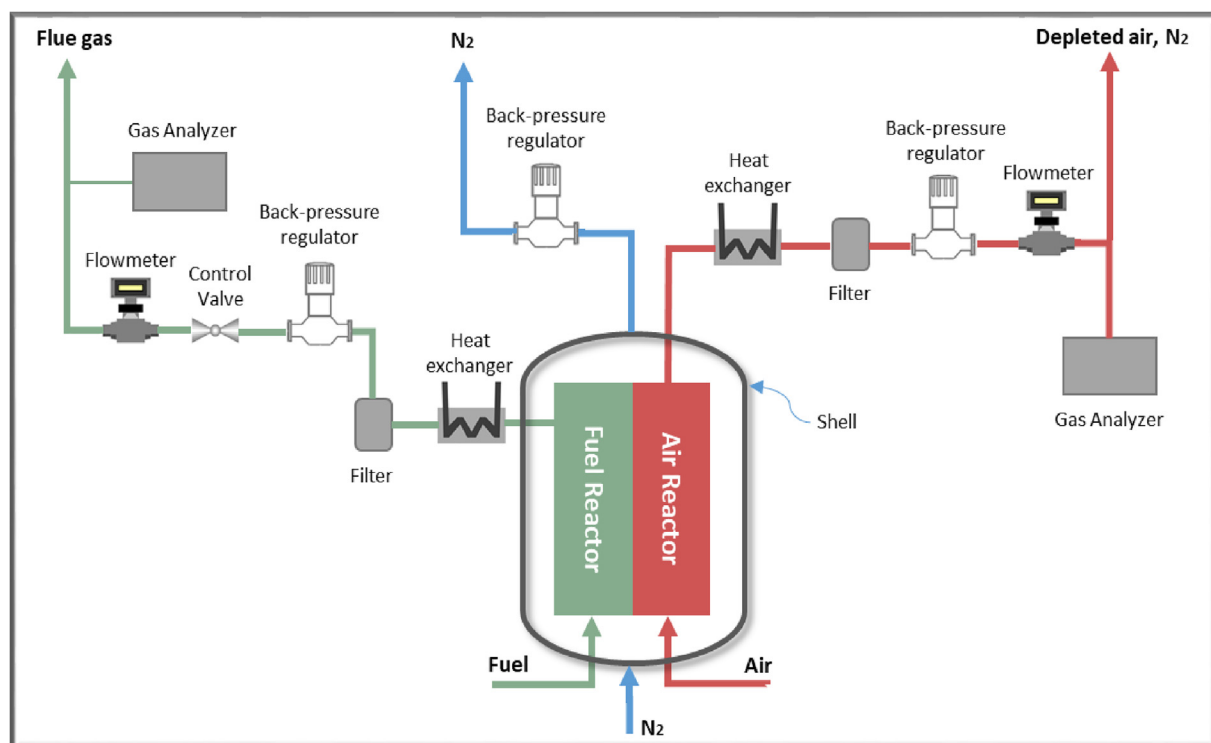


Fig. 2. A simplified illustration of the ICR auxiliary components.

collect any elutriated fine particles. A gas analyzer (from ETG Risorse e Tecnologia) used to measure the dry gas composition from the AR and the FR. The gas analyzer measures multiple gases with a single optical path platform using a non-dispersive infrared sensor for CO and CO<sub>2</sub> measurement and an electrochemical sensor for O<sub>2</sub> measurement. The measurement range for CO, CO<sub>2</sub> and O<sub>2</sub> is 0–30%, 0–50% and 0–25%, respectively. The outlet gas from the FR was diluted with N<sub>2</sub> a known feed rate, first to ensure accurate gas concentration measurement within the gas analyzer measurement range and secondly to determine the molar outlet flow rates of the different species. Back-pressure regulators were installed on the outlet of each reactor chambers and the shell to control the pressure inside the reactor and the shell. Other devices also used to control and monitor the reactor operation, including mass flow controllers for gas feed, flowmeter for gas outlet measurement, thermocouples, pressure sensors and valves. During operation, a small amount of elutriated solids was collected on the filters and the coolers after each section. It should be noted that the attrition rate was low as the selected oxygen carrier has high mechanical and thermochemical stability.

## 2.2. Oxygen carrier

A NiO-based oxygen carrier was used in this study. The OC particles supported on Al<sub>2</sub>O<sub>3</sub> with a NiO/Al<sub>2</sub>O<sub>3</sub> ratio of 65/35 and consisted of around 37% free NiO which are available for reaction (the OC manufactured by VITO). This OC was selected as it revealed high chemical performance and stability for CLC application in many previous studies [23,25,26]. However, a major disadvantage of using a NiO-based OC is its high toxicity. Therefore, extensive health and safety measures are required when handling this OC.

## 2.3. Fuel

CO was the only gaseous fuel used for all PCLC experiments in this study, given its high reactivity with the NiO-based oxygen carrier with a simple reaction mechanism. Hence, the main focus of the study can be concentrated towards understanding the various performance measures of the ICR under high pressure operation. The fuel was also diluted with N<sub>2</sub> in some cases to maintain the flowrate in the FR at a certain level while maximizing fuel conversion. In several cases, particularly at elevated pressures, solids circulation was not sufficient to fully convert a pure fuel stream fed at a fluidization velocity required for good ICR operation, thus requiring the fuel to be diluted with N<sub>2</sub>.

## 2.4. Experimental procedure

Experiments were conducted by altering four independent variables: solids inventory, pressure, air fluidization velocity in AR and fuel fluidization velocity in FR. Four dependent variables were determined from each experiment: solids circulation rate, CO conversion, CO<sub>2</sub> capture efficiency and CO<sub>2</sub> purity. The FR reactor temperature during CLC operation was maintained constant at around 840 °C for all the cases by controlling the power output of the electrical heater surrounding the reactor. During autothermal PCLC operation, the electrical heater was switched off, hence the temperature inside the reactor was maintained only by the oxygen carrier circulation. Table 1 shows a summary of the main operating conditions examined in the current study. The experimental results for each case were averaged over at least one hour of steady state CLC operation.

## 2.5. Data evaluation

### 2.5.1. Fuel conversion

CO conversion during CLC operation ( $\gamma_{CO}$ ), was defined as in Eq. (1) where  $F_i$  and  $F_o$  refer to the inlet and outlet molar rates respectively:

$$\gamma_{CO} = \frac{F_{iCO} - F_{oCO}}{F_{iCO}} \times 100 \quad (1)$$

### 2.5.2. CO<sub>2</sub> capture efficiency and purity

The gas leakage between the AR and FR is characterize by the CO<sub>2</sub> capture efficiency and purity. CO<sub>2</sub> capture efficiency is calculated based the amount of CO<sub>2</sub> leaking to the AR outlet according to Eq. (2) and the CO<sub>2</sub> purity is calculated based on amount of air leaking to the FR outlet as in (Eq. (3)).

$$\text{CO}_2 \text{ capture efficiency} = \left(1 - \frac{F_{AR,OCO_2}}{F_{FR,iCO}}\right) \times 100 \quad (2)$$

$$\text{CO}_2 \text{ purity} = \left(\frac{F_{FR,oCO_2} + F_{FR,oCO}}{F_{FR,o_{tot}} - F_{FR,iN_2}}\right) \times 100 \quad (3)$$

### 2.5.3. Solids circulation rate

The solids circulation rate is the prime CLC criterion because the solids transfer oxygen and heat between AR and FR reactors fulfilling the required heat and mass balance. In the current study, the solids circulation rate was estimated by an indirect approach considering the correlation between the solids conversion difference between AR and FR and the solids circulation rate. After each steady state CLC operational case, the OC was re-oxidized by replacing the fuel feed on the FR by N<sub>2</sub>, while measuring the O<sub>2</sub> concentration in the AR outlet. This strategy gives the O<sub>2</sub> consumption of the reduced OC in the reactor, which reveals the degree of reduction of the OC of the previous CLC operation, which is directly linked with the solids circulating rate.

The solids conversion difference was calculated based on the total O<sub>2</sub> consumption ( $m_{O_2}$ ) from the re-oxidation test, as follows:

$$\Delta X_s = X_{s,AR} - X_{s,FR} \quad (4)$$

$$X_s = \frac{m_{OC} - m_{OC,ox}(1 - R_o)}{m_{OC,ox}R_o} \quad (5)$$

$$m_{OC} = m_{OC,ox} - m_{O_2} \quad (6)$$

The solids conversion difference ( $\Delta X_s$ ) was calculated combining Eqs. (4), (5) and (6) and by assuming that the OC mass in the AR was equal to that in the FR, and the O<sub>2</sub> consumption from the re-oxidation test was only from the reduced OC placed in the FR, considering that the OC placed in the AR was fully oxidized ( $X_{s,AR} = 1$ ); since air was supplied to the AR in excess. Accordingly, the solids circulation rate calculated from the oxygen balance in the AR as in Eq. (7).

$$F_{O_2,AR,in} x_{O_2} M_{O_2} = \dot{m}_s R_o \Delta X_s \quad (7)$$

This approach was adopted by various CLC studies carried out in a circulating fluidize-bed reactor [27–34] and it was adopted in the previous ICR atmospheric operation study [24].

### 2.5.4. The oxygen carrier to fuel ratio (OC/fuel ratio, $\phi$ )

The oxygen carrier to fuel ratio, defined as the ratio between the

**Table 1**  
Operating condition investigated in this study.

Parameter	Value
Temperature (°C)	800–850
Pressure (bar)	1.0–6.0
Solids inventory (kg)	2.0 and 2.5
Fluidization velocity in AR (m/s)	0.45–0.80
Fluidization velocity in FR (m/s)	0.055–0.13
Volumetric flowrate in AR (NL/min)	35–210
Volumetric flowrate in FR (NL/min)	8.5–40
Total time of CLC operation (hr)	~40
Thermal power of the fuel input	1–4 kW

flow of oxygen supplied by the oxygen carrier and the oxygen needed for complete CO conversion, is calculated by Eq. (8) as follows:

$$\phi = \frac{\dot{m}_s R_o X_{s,AR}}{0.5 \dot{n}_{CO} M_{O_2}} \quad (8)$$

### 2.5.5. The overall air equivalence ratio ( $\lambda$ )

The overall air equivalence ratio ( $\lambda$ ) compares the oxygen fed to the AR with the oxygen demand for complete combustion of the fuel fed to the FR. Lowering the air equivalence ratio is done by reducing the amount of air fed to the AR. The definition of the air equivalence number is shown in Eq. (9):

$$\lambda = \frac{0.21 F_{air,in}}{0.5 F_{CO,in}} \quad (9)$$

### 2.5.6. Uncertainties of the measurements

The accuracies of the measuring devices used in this study (provided by the manufacturer) are as follows:  $\pm 0.5\%$ ,  $\pm 1\%$ ,  $< \pm 0.5\%$ ,  $< \pm 0.5\%$ , and  $< \pm 3\%$  for mass flow controllers, gas flowmeters, thermocouples, pressure sensors and the gas analyzer, respectively. The highest uncertainty is associated with the gas concentration measurements. However, this uncertainty was mitigated by operating each experimental cases for at least 1 hr of steady state CLC operation, and average data of these measurements were taken as representative.

In addition, the methodology of estimating the solids circulation rate (described in Section 2.5.3) involves some important uncertainties, primarily the assumptions that the oxygen carrier is equally distributed between the two reactor sections and fully oxidized in the air section. It was not possible to accurately quantify this uncertainty, but it should be similar between the different cases, implying that the response of solids circulation rate to various independent variables reported in the results section should be reliable. Moreover, two of the experimental cases were repeated two times and resulted in a deviation no larger than 5%, confirming that the reported results are reliable.

## 2.6. Scope of the study

The focus in this study is on understanding the role played by the pressure, the solids inventory and the fluidization velocity in AR and FR on various ICR performance measures during chemical looping combustion condition. The ICR performance measures include CO<sub>2</sub> capture efficiency and purity, fuel conversion, and solids circulation rate. The collected data will also give the basis for designing an ICR pilot plant in the order of 0.1 to 1 MW at pressures relevant to real industrial conditions by extracting a correlation linking the solids circulation rate to the process variables such as the fluidization velocity in the two chambers, the operating pressure and the solids inventory.

## 3. Results and discussions

The results will be presented and discussed in two main parts: 1) the ICR operation performance under pressurized CLC conditions and its sensitivity to the process variables and 2) fitting the collected data into a correlation for solids circulation rate. Table 2 and Table 3 summarize the main results of the PCLC experimental campaigns for the operation with 2.5 kg and 2 kg solids loading, respectively, which will be discussed in the following sections.

### 3.1. Pressurized chemical looping combustion (PCLC)

Fig. 3 shows an example of the gas concentration profile of the outlet gases from the FR and AR during PCLC at 4 bar (case-11). A relatively constant CO<sub>2</sub> concentration in the FR and stable consumption of O<sub>2</sub> in the AR was attained during a steady state CLC operation. This

**Table 2**  
Summary of the main results of the CLC experimental campaigns using 2.5 kg of solids inventory.

Experimental cases	Pressure	Flowrate Lm/min		Products Concentration vol%						CO conversion %	CO <sub>2</sub> Capture Efficiency %	CO <sub>2</sub> Purity %	Solids circulation g/s	The air equivalence ratio	The OC/Fuel ratio		
		FR		FR		AR		AR									
		air	CO	N <sub>2</sub>	CO	CO <sub>2</sub>	O <sub>2</sub>	N <sub>2</sub>	CO <sub>2</sub>							O <sub>2</sub>	N <sub>2</sub>
1	1	35	10	0	0.27	92.24	1.31	6.19	2.36	8.07	89.58	99.73	92.92	92.5	2.78	1.47	1.81
2	2	40	10	0	0.21	92.63	1.09	6.06	2.24	9.97	87.79	99.79	92.15	92.84	2.96	1.68	1.93
3	3	60	10	0	0	91.98	1.05	6.97	1.34	13.96	84.7	100	92.66	91.98	3.81	2.52	2.49
4	4	73	5	3.5	0.03	54.17	0.9	44.9	0.56	18.22	81.22	99.95	92.15	92.14	4.36	6.13	5.70
5	5	80	15	0	5.99	86.48	0.39	7.14	1.63	13.55	84.82	94.01	92.06	92.47	3.18	2.24	1.38
6	6	100	15	0	0.2	92.74	0.64	6.43	1.22	14.68	84.11	99.8	92.5	92.94	3.68	2.80	1.60
7	7	110	8	5	0	56.55	0.55	42.9	0.58	18.04	81.38	100	92.32	91.89	3.91	5.78	3.19
8	8	120	15	5	1.29	68.09	0.69	29.93	1	15.85	83.16	98.27	92.5	92.51	3.42	3.36	1.49
9	9	105	15	5	5.1	64.17	0.61	30.12	1.19	15.43	83.37	93.19	92.2	92.36	3.14	2.94	1.36
10	10	140	15	5	0.12	69.02	0.7	30.16	0.89	16.54	82.57	99.84	92.12	92.19	3.73	3.92	1.62
11	11	160	15	10	0.22	55.52	0.46	43.8	0.78	17.1	82.12	99.63	92.09	92.9	3.60	4.48	1.57
12	12	160	15	25	0.92	33.37	0.52	65.19	0.74	17.26	81.99	97.55	92.43	91.45	3.37	4.48	1.47
13	13	165	12	8	0.05	55.17	0.7	44.08	0.57	18.06	81.37	99.92	92.46	92.03	3.73	5.78	2.03
14	14	165	20	0	8.87	83.96	0.91	6.27	1.01	16.39	82.6	91.13	92.11	92.83	3.73	3.47	1.22
15	15	200	15	10	0	55.46	1.19	43.35	0.63	17.91	81.46	100	91.86	92.43	3.77	5.60	1.64
16	16	200	15	0	0	92.29	0.89	6.82	0.6	17.88	81.52	100	92.32	92.29	3.98	5.60	1.73
17	17	175	15	10	1.89	53.4	0.71	44	0.72	17.56	81.72	96.85	91.93	92.15	3.48	4.90	1.52
18	18	210	15	10	0	55.48	1.09	43.43	0.55	18.06	81.39	100	92.58	92.47	3.66	5.88	1.59

**Table 3**  
Summary of the main results of the CLC experimental campaigns using 2 kg of solids inventory.

Experimental cases	Pressure	Flowrate (Ln/min)		Products Concentration (vol%)						CO conversion %	CO <sub>2</sub> Capture Efficiency %	CO <sub>2</sub> Purity %	Solids circulation g/s	The air equivalence ratio	The OC/Fuel ratio
		AR	FR	FR	FR	FR	FR	AR	AR						
19	1	40	7	3	0.25	67.39	0.38	31.97	0.47	13.5	86.03	99.64	2.37	2.40	2.41
20	2	80	8	7	1.32	50.76	0.27	47.65	0.3	17.01	82.68	97.52	2.55	4.20	2.27
21	3	120	8	12	0.37	38.48	0.22	60.93	0.22	18.36	81.42	99.09	2.76	6.30	2.46
22	23	120	8	7	0.51	51.06	0.23	48.2	0.21	18.3	81.49	99.04	2.89	6.30	2.57
23	22	120	9	11	0.9	43.01	0.25	55.84	0.23	18.01	81.76	98	-	5.60	-
24	24	130	9	11	0.1	43.83	0.28	55.8	0.19	18.17	81.64	99.78	2.92	6.07	2.31
25	4	160	9	16	0.36	34.62	0.36	64.66	0.18	18.73	81.1	99.01	3.12	7.47	2.47
26	160	11	14	14	2.59	40.3	0.45	56.66	0.2	18.47	81.33	94.11	-	6.11	-

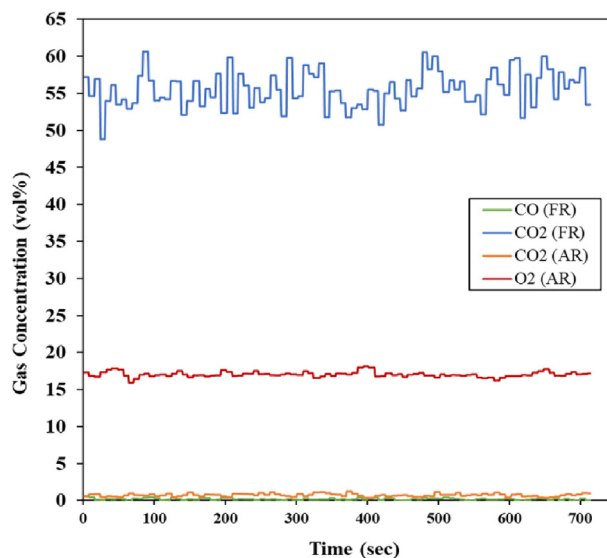


**Fig. 3.** Gas product concentration measured at the FR and AR outlet during PCLC tests (case-11).

demonstrates the ability of the ICR reactor in achieving a stable solids circulation between the two chambers.

Further sensitivity study of ICR performance under pressurized CLC conditions (PCLC) will be presented and discussed in this section, with the focus on the 2.5 kg of solids inventory. The respective experiments were conducted in a pressure range of 1 to 6 bar, where air flowrate to the AR was increased proportionally to the pressure in order to maintain the gas fluidization velocity constant. The volumetric gas flowrate to the FR was increased with pressure; however, the gas fluidization velocity was decreased to avoid solids elutriation due to large bed expansion. This decrease should however have a limited effect on the ICR performance as found in the atmospheric study [24]. This is also confirmed in the current study where an increase of 60–66% in the FR flow rate has barely resulted in 5–6% decrease in solids circulation rate (cases 11 and 12 at 4 bar and cases 15 and 16 at 5 bar;  $U_{AR}$  was maintained constant for each operating pressure). Increasing the fluidization velocity in the AR ( $U_{AR}$ ) resulted in higher solids circulation rate at different pressure as illustrated in Fig. 4. As explained in the

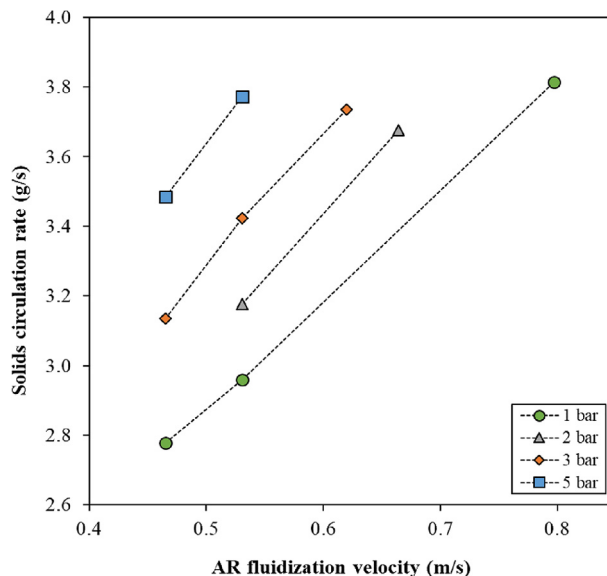


**Fig. 4.** Solids circulation rate as function of air fluidization velocity in AR at various pressure.

previous study [24], the increase in  $U_{AR}$  leads to larger bed expansion, thus resulting in larger solids entrainment to reach the freeboard and fall into the FR through the top port. The larger accumulation rate of solids in FR creates larger driving force for solids to flow back from the FR to the AR through the bottom port. The  $CO_2$  separation performance remains relatively insensitive to both AR and FR flowrates (Table 3).

### 3.1.1. Effect of pressure

The understanding of the effects of pressure on fluidized-beds performance is essential for optimal design and operation. The operating pressure mainly affects the hydrodynamic behavior of the fluidized-beds through the increase of the gas density, which increases the gas-solids drag [35]. Solid-solid interactions are not directly changed with elevated pressure due to the rigidity of the solids [36], but a denser gas increases the gas-particle drag, which also leads to fewer solid-solid collisions. As a result, it produces a more homogeneous fluidization and decreases the minimum fluidization velocity [37,38]. Increasing pressure also increases the bed-expansion and reduces the bubble size; as a result it leads to a better gas-solid contact and therefore higher inter-phase mass-transfer [39,40].

Fig. 5 shows the results of solids circulation rate,  $CO_2$  capture efficiency and purity for the two AR fluidization velocities ( $U_{AR} = 0.53$  and  $0.46$  m/s) as function of the operating pressure. The solids circulation rate was found to increase with the pressure. Similar observation for the increases of solids circulation rate with pressure have been reported by several studies on pressurized circulating fluidized-bed [41,42]. For instance, Horio et al. [41] carried out a hydrodynamic investigation on a pressurized circulating fluidized bed using FCC particles in a pressure range of 1 to 7 bar. They found that, keeping the gas velocity constant with pressure increases the solids circulation rate and that a lower gas velocity is required for the transition from bubbling to turbulent fluidization regimens when the pressure is increased. This result stems from the fact that the gas density increases with pressure, which increases the gas-solids drag [43,44].

Acceptably high  $CO_2$  capture efficiency and purity were established (~92%) for all cases independently of the pressure for both tested AR fluidization velocities (Fig. 5). The insensitivity of undesired gas mixing to both the AR feed rate and the pressure supports previous findings that gas transport with the circulating solids between the two reactor sections is not the main gas mixing mechanism in this particular ICR setup [24]. In an optimal ICR system, as would be designed during

further scale-up efforts toward commercial deployment, the gas would only leak with the circulating solids in a ratio of about 1:1 by volume, resulting in substantially lower leakage than observed in Fig. 5 (see previous large-scale simulation studies [45,46]). Considerable room for further reductions in gas leakage therefore exists by optimising the ICR port design and operating conditions. As discussed in the next section, the 2 kg inventory offers an indication of the good separation performance that can be achieved in an ICR. If required, the ports can be designed to act like loop seals by injecting steam into the ports to further reduce the gas leakages.

To identify a condition at which similar hydrodynamic performance can be obtained at various pressures, additional experiments were conducted at lower pressures (1, 2, and 3 bar) with higher AR fluidization velocities (case-3, 6, and 10). Fig. 6a shows that both AR fluidization velocity and pressure led to an increase in the solids circulation rate. To obtain a similar solids circulation rate at various pressures, different AR fluidization velocities are needed. For instance, to achieve a solids circulation rate of 3.6 g/s, the required AR fluidization velocity can be interpolated from the data in Fig. 6a and b shows that the required air fluidization velocity for achieving a given solids circulation rate decreases with increasing the pressure.

### 3.1.2. Effect of solids inventory

The solids inventory is a critical operating variable for the CLC process. In CLC, the solids inventory must be high enough to achieve complete fuel conversion. A more reactive oxygen carrier is advantageous, since lower solids inventory can be used, which will reduce the required reactor size and pressure drop. For ICR, the solids inventory also has a strong influence on the hydrodynamic behaviour of the system [24].

To study the effects of the solids inventory on ICR performance, an additional experimental campaign was conducted using 2 kg of solids inventory over a pressure range of 1 to 4 bar (Table 3), to be compared with the results using 2.5 kg of solids inventory discussed in the previous sections. AR and FR flowrates were maintained similar to the experimental cases with 2.5 kg of solids inventory for each pressure, to focus the study on the effects of solids inventory.

Fig. 7 reveals the effect of increasing the solids inventory on the solids circulation rate at different pressures. Both solids inventories showed a similar trend of increasing the solids circulation rate with pressure. The addition of more solids to the ICR system leads to higher

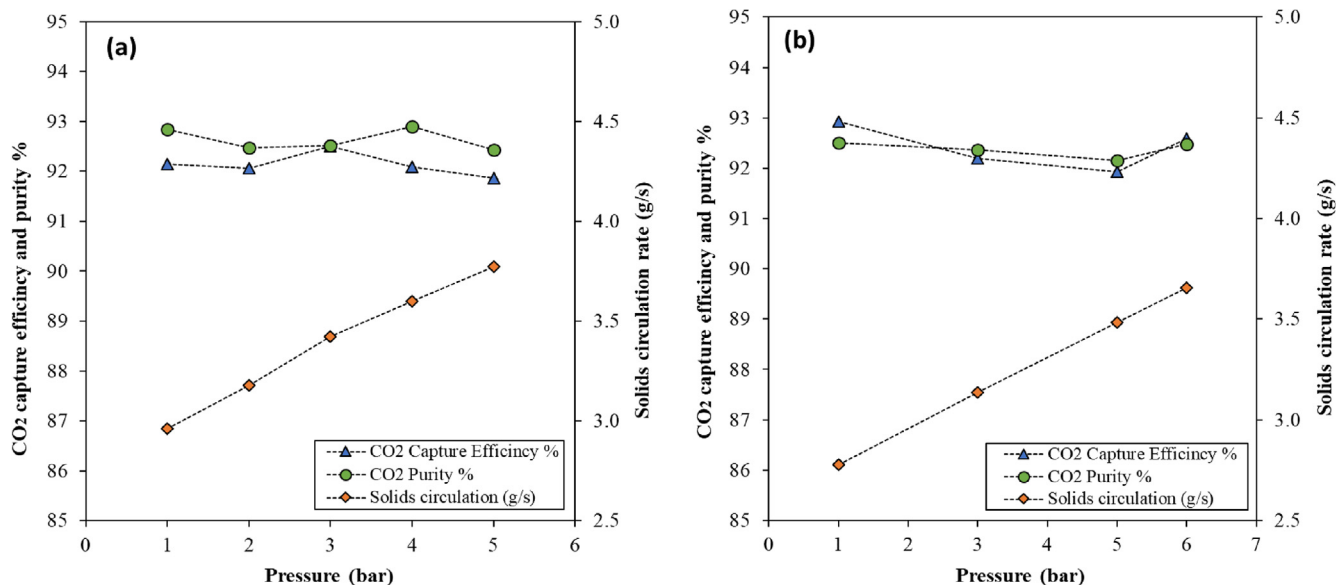


Fig. 5. Solids circulation rate and  $CO_2$  capture efficiency and purity % as function of pressure, a)  $U_{AR} = 0.53$  m/s, case (2,5,8,11,15), b)  $U_{AR} = 0.46$  m/s, case (1,9,17,18).

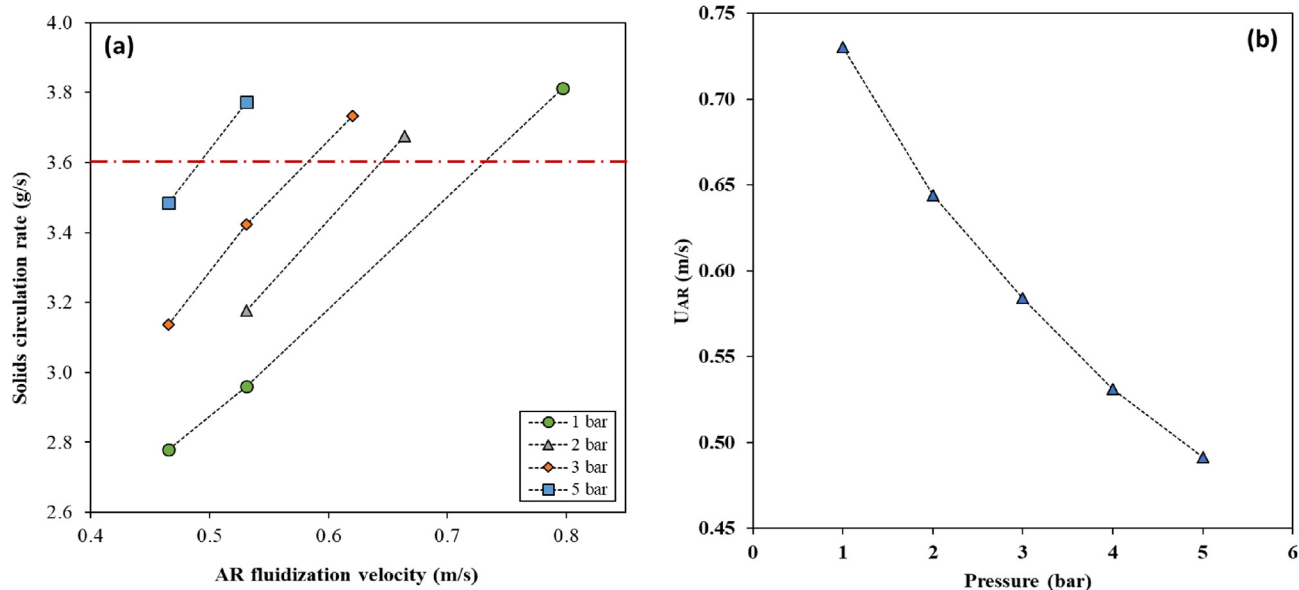


Fig. 6. a) Solids circulation rate as function of air fluidization velocity in AR at various pressure, b) the estimated air fluidization velocity in AR as function of pressure that keep solids circulation rate constant at 3.6 g/s.

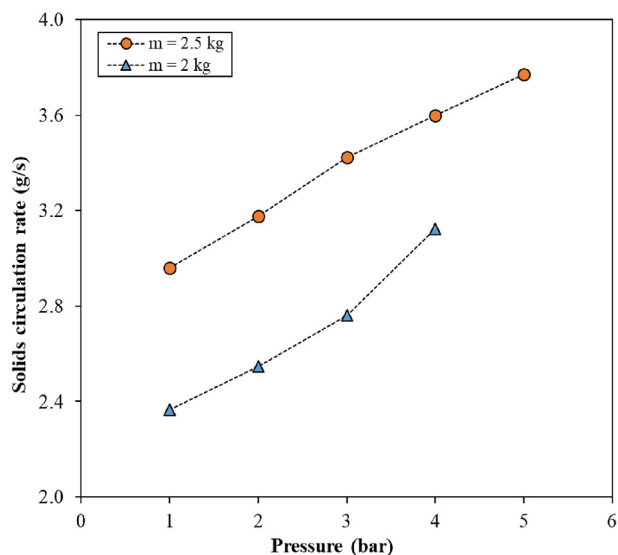


Fig. 7. Solids circulation rate as function of pressure for various solids inventories (2 and 2.5 kg),  $U_{AR} = 0.53$  m/s, case (2,5,8,11,15) compared with case (19,20,21,25).

solids circulation rates (an increase of 25% in the solids inventory has resulted in a solids circulation increase of  $\sim 30\%$ ). The bed expansion in the AR is the main driving force for transporting the solids to the freeboard to reach the top port for circulation from the AR to the FR. A larger bed inventory allows for greater bed expansion, thus increasing the solids circulation rate.

The effect of solids inventory and pressure on CO<sub>2</sub> capture efficiency and purity during CLC operation are shown in Fig. 8. It is shown that for both solids inventory the pressure has no effect on CO<sub>2</sub> capture efficacy and purity. However, high CO<sub>2</sub> capture efficiency and purity ( $\sim 97\%$ ) was observed using lower solids inventory (2 kg), compared to around 92% for the higher solids inventory (2.5 kg). A similar effect of increasing gas leakage between the two chambers with increasing solids inventory was also observed at atmospheric pressure [24]. As outlined in that study [24], this effect is mainly due to design and hydrodynamic constrains of the ICR system. The most likely explanation is that higher solids inventories cause larger instantaneous pressure fluctuations at

the bottom of the two reactor sections, resulting in short-lived backwards and forwards gas flows through the bottom port (in addition to the gas flowing from the FR to the AR with the solids). These results suggest that this mechanism for extra undesired gas mixing remains strong at 2.5 kg of solids inventory, but almost disappears at 2 kg of solids inventory. Improved design of the bottom port and optimal solids loading should therefore be prioritized during scale-up of the ICR concept.

### 3.1.3. Effect of the operating conditions on fuel conversion

In this section, the effect of various operating variables on the fuel conversion is discussed. Fig. 9 shows the effect of air flowrate and pressure on CO conversion, increasing both air flowrate and pressure improve the CO conversion as a result of increasing the solids circulation rate. Fig. 10a illustrates the effect of solids circulation rate and OC/fuel ratio on CO conversion for various cases at constant fuel feed (CO

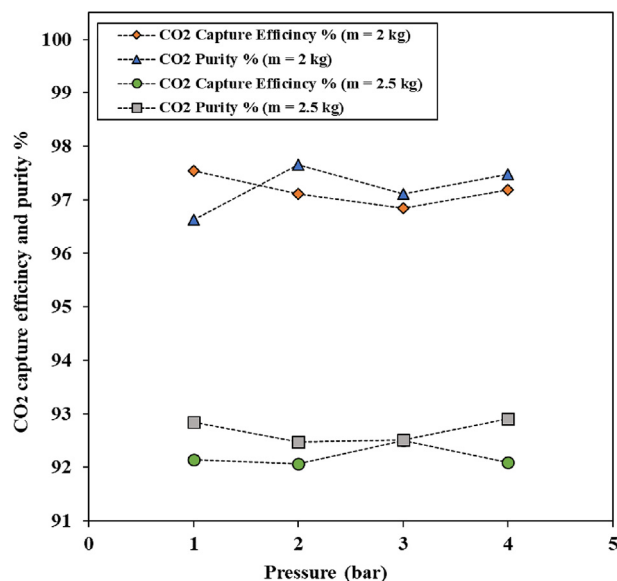


Fig. 8. CO<sub>2</sub> capture efficacy and purity % as function of pressure for various solids inventory (2 and 2.5 kg),  $U_{AR} = 0.53$  m/s, case (2,5,8,11,15) compared with case (19,20,21,25).

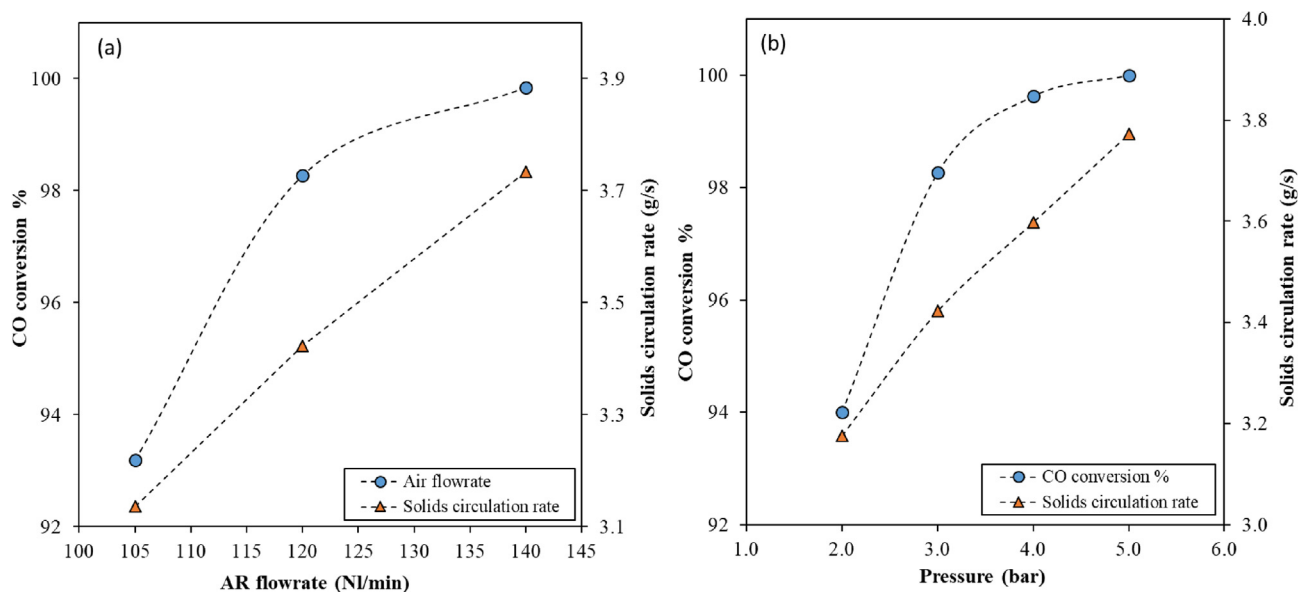


Fig. 9. a) Effect of AR flowrate on CO conversion and solids circulation rate, (Pressure = 3 bar). b) Effect of pressure on CO conversion and solids circulation rate, (FR specific inventory = 393 kg/MW).

flowrate = 15 NI/min) and solids inventory of 2.5 kg (overall specific inventory = 787 kg/MW). It can be seen that complete CO conversion was achieved with solids circulation rate higher than 3.6 g/s and OC/fuel ratio higher than 1.55. When using 2 kg of solids inventory, a higher OC/fuel ratio was required (higher than 2.3) to achieve complete CO conversion compared to the results of 2.5 kg of solids inventory (Fig. 10b). This effect is due to the short bed height that led to a smaller gas residence time in the bed, which reduces the gas-solids contact quality, thus negatively affecting CO conversion. The current ICR setup accentuates this effect because the gas is injected using a perforated cylindrical tube in a relatively concentrated manner, imposing significant bubble-to-emulsion mass transfer limitations. The specific solids inventory (937–1472 kg/MW) is higher than the cases with 2.5 kg solids inventory because a lower CO feed had to be used to

get good conversion due to the lower solids circulation rates in the 2 kg solids inventory cases. However, the total fuel reactor flowrate was kept similar using greater  $N_2$  dilution, explaining the higher OC/fuel ratio required for full conversion despite the higher specific solids inventory.

### 3.2. Correlation for the solids circulation rate

The experimental data of this study have revealed that the solids circulation rate ( $G_s$ ) in the ICR reactor is affected mainly by four independent variables: solids inventory ( $m_s$ ), pressure ( $P$ ), air fluidization velocity in AR ( $U_{AR}$ ) and fuel fluidization velocity in FR ( $U_{FR}$ ). To better understand the ICR operation at different conditions, the obtained solids circulation rates from the different experiments have been correlated with the four independent variables using the following empirical

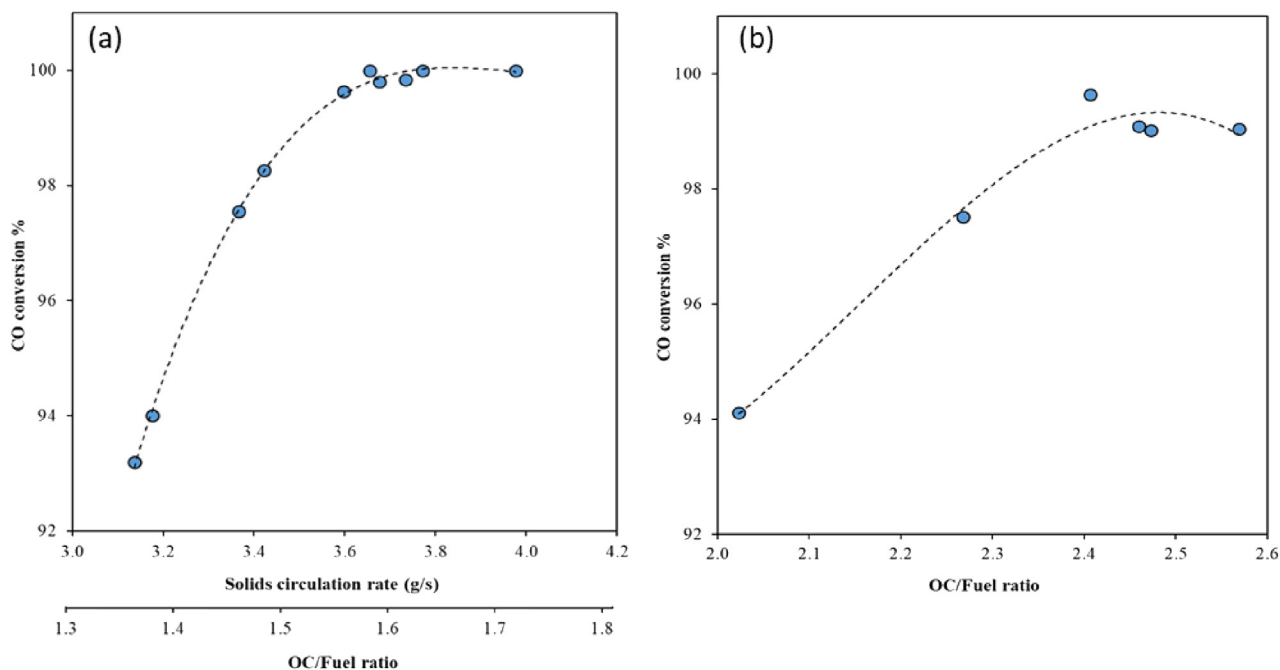


Fig. 10. a) CO conversion with different solids circulation rate and OC/fuel ratio, (solids inventory = 2.5 kg), b) CO conversion with different OC/fuel ratio, (solids inventory = 2.0 kg).

correlation:

$$G_s = a m_s + b P + c U_{AR} + d U_{FR} + e \quad (10)$$

The correlation was evaluated using the non-linear regression method of Wolfram Mathematica. This proposed linear correlation is the simplest model possible from four independent variables. More complex correlations using additional model exponents to account for any non-linear influence of the four independent variables on the solids circulation rate were also evaluated, but this resulted in negligible improvement over the linear relationships shown in Eq.(10). The accuracy of the obtained correlation is judged by the correlation coefficient  $R^2$ , and the significance levels of the interaction terms were diagnosed by the P-value (the probability value) obtained from the analysis of variance (ANOVA). The P-value is the probability that the observed effect is simply random. Hence, the smaller the P-value, the more significant the observed effect. The values of the model parameters in Eq.(10) along with their corresponding 95% confidence limits (CLs) and P-Values are shown in Table 4. As can be seen in Fig. 11, the predicted solids circulation rate by the correlation fits the experimental data well. The correlation coefficient  $R^2$  has a very high value of 0.9997, indicating that almost no further improvement can be gained from more complex correlations.

Among the four independent variables,  $U_{AR}$  shows the lowest P-value (Table 4), which means that the AR fluidization velocity is the most significant variable affecting the solids circulation rate. Based on the P-values, the four parameters of Eq. (10) affect the solids circulation rate with the following significance order:  $U_{AR} > m_s > P > U_{FR}$ . This result is expected given that the air fluidization velocity and the solids inventory are the main driving forces for lifting solids to the top port for circulation from the AR to the FR.

Applying the developed correlation (Eq. (10)), a sensitivity analysis was carried out to gain further insight into the effects of the various independent variables on the solids circulation rate. It should be noted that the correlation was applied with some extrapolation, which could involve some uncertainty. The various independent variables were changed by  $\pm 50\%$  from a reference values ( $m_s = 2.5$  kg,  $P = 5$  bar,  $U_{AR} = 0.53$  m/s,  $U_{FR} = 0.13$  m/s), while the solids circulation rate was evaluated using the developed correlation. Fig. 12 shows that increasing the solids inventory, pressure and  $U_{AR}$  resulted in an increase on the solids circulation rate, whereas increasing  $U_{FR}$  slightly decreased the circulation rate. A possible explanation for the small effect of  $U_{FR}$  is that the denser fuel reactor bed created by lower fluidization velocities leads to a more consistent presence of solids at the top of the bottom port, slightly increasing the circulation rate. Interestingly, Fig. 12 shows that the effect of solids inventory is considerably larger than that of air reactor velocity, even though the P-value of  $U_{AR}$  was lower than that of  $m_s$  (Table 4). Since only two different solids inventories were evaluated in the experiments, this effect involves more uncertainty than the others.

For practical application of ICR for PCLC, it will be beneficial to increase the gas mass flowrate in both FR and AR proportionally to the pressure, which would lead to a smaller reactor size for a given fuel input. However, as it has been observed from the current study, the solids circulation rate does not increase proportionally to the pressure in ICR, which will eventually lead to insufficient oxygen carrier circulation for converting the incoming fuel. Tuning the other process variables such as the solids inventory and the  $U_{AR}$  would be necessary if the mass flow rate to the FR is to be increased proportionally to the

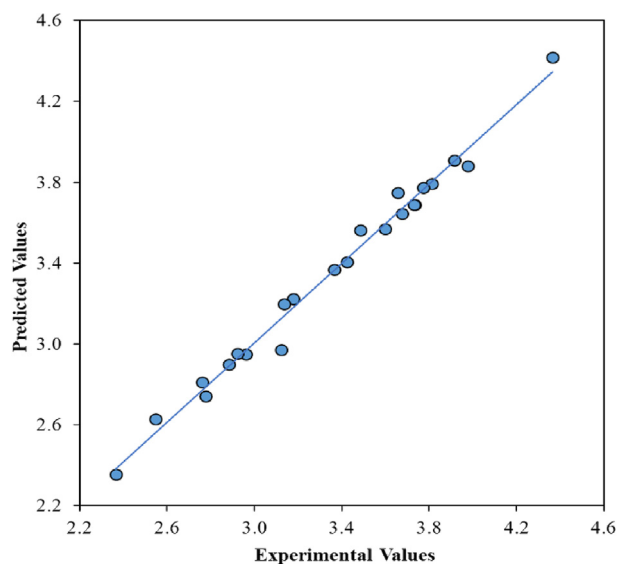


Fig. 11. Reconciliation plot between predicted and experimental solids circulation rate.

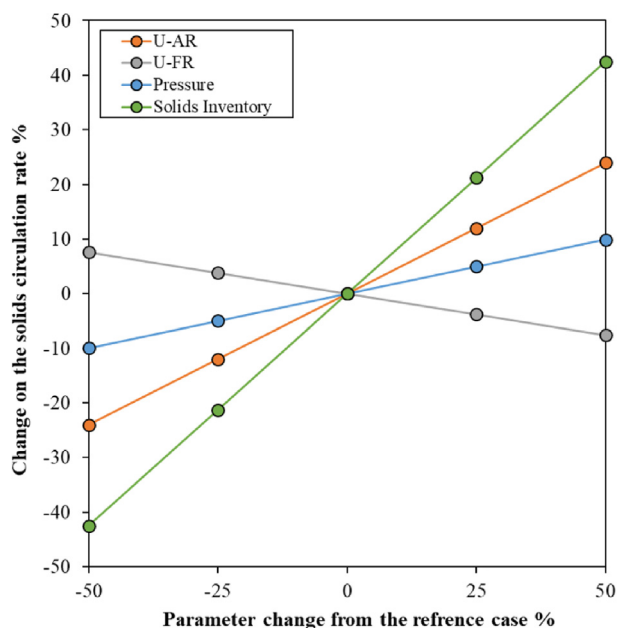


Fig. 12. Sensitivity analysis for the effects of the various independent variables on the solids circulation rate.

pressure.

An example of the adjustment to the process variables that should be applied at pressurized operation is illustrated by the following example. To achieve complete fuel conversion in ICR for 4 kW of thermal power of CO as fuel; the required solids circulation rate is around 4.0 g/s. This value is approximated based on the experimental case-22, in which the fuel conversion was 91% at a solids circulation rate of 3.7 g/s and a thermal power of CO feed of 4 kW (Table 2). Using the developed correlation (Eq.(10)), Fig. 13 shows the required air fluidization

Table 4

Estimated parameters (at 95% confidence limit) and P-value for the correlation of solids circulation rate (Eq. (10)).

	a	b	c	d	e
Estimated value	1.19 $\pm$ 0.14	0.14 $\pm$ 0.04	3.17 $\pm$ 0.29	-4.02 $\pm$ 1.83	-1.32 $\pm$ 0.34
P-Value	3.5E-13	3.2E-7	9.9E-15	0.0002	1.8E-6

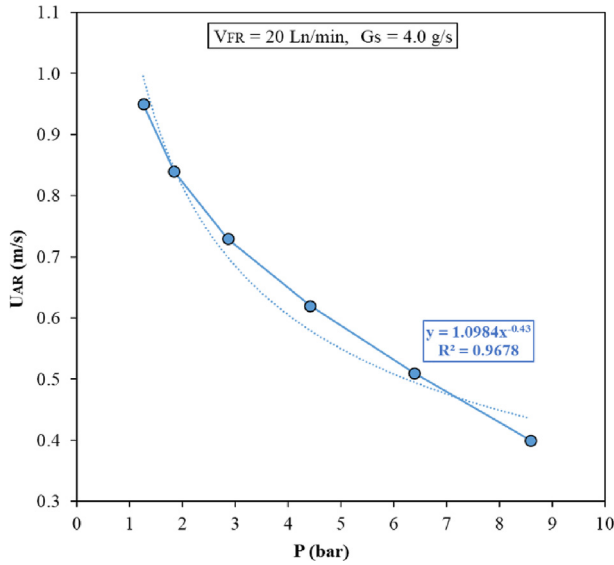


Fig. 13. Predicted  $U_{AR}$  as function of pressure at a constant solids circulation rate and thermal power of the fuel.

velocity  $U_{AR}$  at various pressures and at constant thermal power of CO input (4 kW) and constant solids circulation rate (4.0 g/s). It can be observed that the required  $U_{AR}$  decreases with increasing pressure (at which the volumetric flowrate of the fuel ( $V_{FR}$ ) is maintained constant), which can be expressed by the following correlation:

$$U_{AR} = 1.1 P^{-0.43} \quad (11)$$

This result indicates that, to achieve a good operation at constant fuel power at higher pressures, the operation of ICR is possible at lower air fluidization velocity. A similar relationship between pressure and fluidization velocity was revealed by the work of Horio et al. [41] on PCFB; they found that, with similar solids circulation rate, the fluidization velocity scales with pressure as  $U \propto P^{-0.3}$ . It is noted, however, that another important constraint in CLC reactors is imposed by the ratio of air to fuel flowrate. In this example, even though the air fluidization velocity is reduced with pressure, the air mass flow rate increases by a factor of 3 from 1 to 7 bar if the reactor geometry is kept constant. This large increase in air flowrate relative to fuel flowrate will extract more heat and cool the reactor far below the desired operating temperature. Therefore, successful CLC operation will require changes to the cross-sectional area of the AR to also keep the fuel to air mass flow ratio constant.

The use of the fluidization regime diagram of Grace [47,48] provides additional insight for the effect of pressure on the flow regimes in ICR. Fig. 14 displays the fluidization regime at various pressures for the same conditions shown in Fig. 13. It can be seen that, in the AR, increasing the pressure shifts the behaviour slightly toward a more dilute phase. Although  $U_{AR}$  is reduced with increasing the pressure, the air density is strongly increased, increasing the gas-particle drag and shifting the flow regime toward the turbulent fluidization regime ( $U_c$ ). This result is line with the work of Grace et al. [49] and Horio et al. [41], in which they found that with increasing the pressure, a lower superficial gas velocities and higher gas mass flowrates is required for the transitions from bubbling to turbulent and fast fluidization regime.

The opposite trend occurs in the FR, since the fuel mass flowrate was held constant; increasing pressure strongly reduces the fluidization velocity, shifting the operating condition towards the minimum fluidization velocity ( $U_{mf}$ ). Naturally, there will be constraints on how low the fluidization velocity in the FR can become before the bed defluidizes or no longer expands sufficiently to reach the top of the bottom port. In addition, optimal reactor design will always strive to maximize the gas fluidization velocity to reduce reactor size.

Finally, an interesting practical application of the scaling of reactor behaviour with pressure can be mentioned: flexible operation of a CLC combined cycle power plant to balance variable wind and solar power. Such future CLC power plants will most likely be operated with added firing with natural gas or hydrogen after the CLC reactors to increase the turbine inlet temperature to the level of state-of-the-art gas turbines for achieving competitive efficiencies [8]. Part-load operation of the gas turbine reduces the turbine inlet temperature (requiring less added firing), as well as the pressure and air flow rate. For example, ramping down a modern HA-class turbine from 100% to 40% load reduces the mass flow rate by 44% and the pressure by 40% [50], keeping the fluidization velocity almost constant. According to the present study (e.g. Fig. 7), a constant fluidization velocity at lower pressure will cause a moderate reduction in solids circulation rate. Such a moderate reduction should not be problematic because the fuel flowrate will be decreased almost proportionately to the air flowrate in part-load operation to keep the reactor outlet temperature constant. Although there are significant uncertainties in using this lab-scale correlation for projecting the performance of a commercial system, this discussion suggests that a future natural gas fired CLC power plant using ICR technology should be able to operate flexibly to balance variable wind and solar power.

### 3.3. Autothermal PCLC operation

Achieving autothermal operation is the primary design criterion of the CLC system. As the overall reaction in CLC systems is highly exothermic, the generated heat should be controlled. The choice of the heat removal will depend on the power generation strategy. For steam cycle applications, which will generally operate at atmospheric pressure, a direct heat extraction from the fluidized bed will result in a higher power plant efficiency and smaller reactor by using an equivalence ratio slightly higher than unity. For pressurized gas turbine applications, the PCLC system will be integrated with the gas combined cycle power plant, therefore, the use of high equivalence ratio will be favoured because the air serves as the primary heat removal mechanism. The higher required air flowrate is justified by the higher power plant efficiency resulting from the downstream combined power cycle.

In the current study, an autothermal CLC operation was achieved at 3 bar (case-8) with the use of an equivalence ratio of 3.4. Fig. 15 shows the temperature profile during autothermal CLC operation of this case.

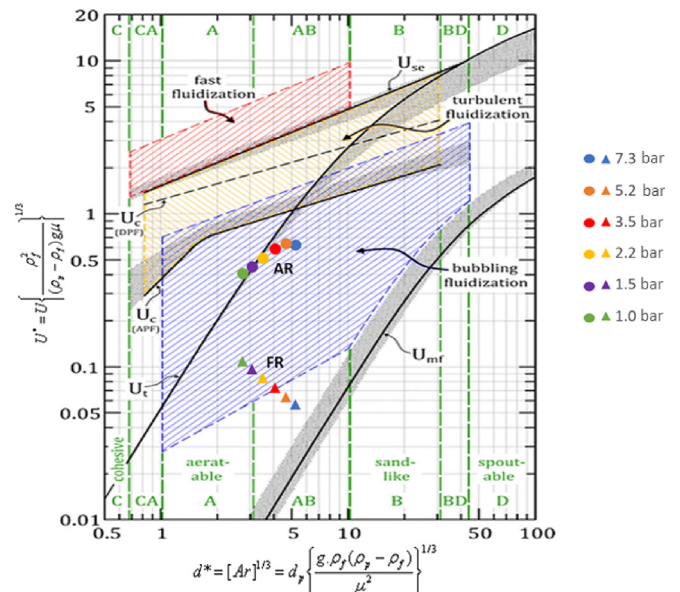


Fig. 14. Fluidization regime of AR (circle) and FR (triangle) under different pressure, the operating condition taken from Fig. 13.

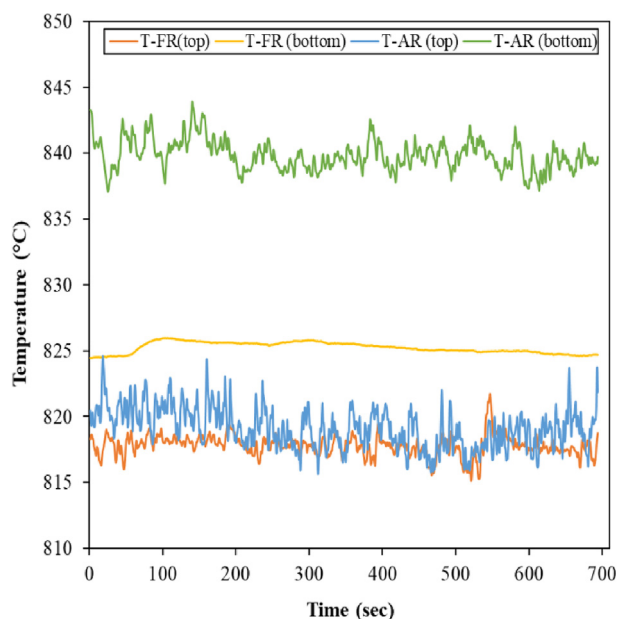


Fig. 15. Temperature profile in FR and AR during an autothermal PCLC test, P = 3 bar, AR flowrate = 120 NL/min, FR flowrate = 20 NL/min, solids inventory = 2.5 kg (case-8).

It can be seen that the temperature measurements was stable at various locations inside the reactor without the use of the external heater. The highly exothermic oxidation reaction in the AR resulted in a higher temperature compared to that in the FR. Increasing the equivalence ratio at higher pressure (4 to 6 bar) removed more heat from the reactor vessel which was compensated by adjusting the power of the electrical heater surrounding the reactor to maintain a constant temperature during CLC operation. The large heat losses from this lab-scale reactor is the main limitation to achieve autothermal operation in the current ICR system. The heat losses would be negligible in an industrial scale ICR; therefore, achieving autothermal operation would be feasible at a higher equivalence ratio, facilitating higher AR fluidization velocities.

#### 4. Summary and conclusions

This study reports the experimental demonstration of an internally circulating reactor (ICR) for pressurized operation of chemical looping-based technologies for minimizing the energy penalty involved in capturing CO<sub>2</sub> from hydrocarbon conversion. Pressurized experiments were completed for chemical looping combustion using CO as fuel and a NiO based oxygen carrier. Stable operation was achieved at pressures up to 6 bar, showing high fuel conversion and sufficiently high CO<sub>2</sub> purity and capture efficiency for all tested operating conditions (92–97%).

In addition to the operating pressure, the effect of other process variables (and their interaction) at elevated pressure, such as fluidization velocities in the air and fuel chambers, as well as the solids inventory, was evaluated. The CO<sub>2</sub> purity and capture efficiency were found to be negatively affected by the solids inventory, independently of the other process variables. The most sensitive performance indicator was the solids circulation rate that was found to increase (by order of influence) with the fluidization velocity in the AR, the solids inventory and the operating pressure, but almost insensitive to the fluidization velocity in the FR. A correlation for solids circulation rate was fitted to the different collected experimental data. The most important insight that could be revealed by the correlation is that, at constant fuel chamber section area, if the fuel mass feed rate is to be increased proportionally to the operating pressure, larger solids inventory and higher fluidization velocity in the AR are required to establish sufficient

solids circulation rate for high fuel conversion.

In the light of the reliable pressurized reactor operation, excellent fuel conversion, and good CO<sub>2</sub> separation performance demonstrated in this study, further scale-up of the ICR concept to 0.1–1 MW<sub>th</sub> pilot plant size for application to pressurized chemical looping can be recommended.

#### Declaration of Competing Interest

The authors declare that they have no known competing financial interests or personal relationships that could have appeared to influence the work reported in this paper.

#### Acknowledgement

The authors would like to acknowledge the financial support of the Research Council of Norway under the CLIMIT program (project number: 255462). The technical support from the thermal engineering laboratory, especially from Mr. Martin Bustadmo, Mr. Paul Svendsen and Dr. Morten Grønli are highly appreciated.

#### References

- [1] IEA (International Energy Agency). World Energy Outlook, Paris; 2018.
- [2] M. Ryden, A. Lyngfelt, T. Mattisson, Synthesis gas generation by chemical-looping reforming in a continuously operating laboratory reactor, *Fuel* 85 (2006) 1631–1641.
- [3] T. Pröll, J. Bolhär-Nordenkamp, P. Kolbitsch, H. Hofbauer, Syngas and a separate nitrogen/argon stream via chemical looping reforming – A 140 kW pilot plant study, *Fuel* 89 (2010) 1249–1256.
- [4] M. Ortiz, L.F. de Diego, A. Abad, F. García-Labiano, P. Gayán, J. Adánez, Hydrogen production by auto-thermal chemical-looping reforming in a pressurized fluidized bed reactor using Ni-based oxygen carriers, *Int. J. Hydrogen Energy* 35 (2010) 151–160.
- [5] H.M. Kvamsdal, K. Jordal, O. Bolland, A quantitative comparison of gas turbine cycles with CO<sub>2</sub> capture, *Energy* 32 (2007) 10–24.
- [6] J. Wolf, M. Anheden, J. Yan, Comparison of nickel- and iron-based oxygen carriers in chemical looping combustion for CO capture in power generation, *Fuel* 84 (2005) 993–1006.
- [7] V. Spallina, M.C. Romano, P. Chiesa, F. Gallucci, M. Van, S. Annaland, G. Lozza, Integration of coal gasification and packed bed CLC for high efficiency and near-zero emission power generation, *Int. J. Greenh. Gas Control* 27 (2014) 28–41.
- [8] M.N. Khan, S. Cloete, S. Amini, Efficiency Improvement of Chemical Looping Combustion Combined Cycle Power Plants, *Energy Technol.* 7 (2019) 1900567.
- [9] M.N. Khan, P. Chiesa, S. Cloete, S. Amini, Integration of chemical looping combustion for cost-effective CO<sub>2</sub> capture from state-of-the-art natural gas combined cycles, *Energy Convers. Manag.* X. (2020) 100044.
- [10] C. Arnaiz del Pozo, S. Cloete, J.H. Cloete, Á. Jiménez Álvaro, S. Amini, The potential of chemical looping combustion using the gas switching concept to eliminate the energy penalty of CO<sub>2</sub> capture, *Int. J. Greenh. Gas Control* 83 (2019) 265–281.
- [11] M. Rydén, A. Lyngfelt, Using steam reforming to produce hydrogen with carbon dioxide capture by chemical-looping combustion, *Int. J. Hydrogen Energy* 31 (2006) 1271–1283.
- [12] L.F. De Diego, M. Ortiz, F. García-Labiano, J. Adánez, A. Abad, P. Gayán, Hydrogen production by chemical-looping reforming in a circulating fluidized bed reactor using Ni-based oxygen carriers, *J. Power Sources* 192 (2009) 27–34.
- [13] P. Ohlemüller, M. Reitz, J. Ströhle, B. Epple, Investigation of chemical looping combustion of natural gas at 1 MW<sub>th</sub> scale, *Proc. Combust. Inst.* 37 (2019) 4353–4360.
- [14] F. Zerobin, S. Penthor, O. Bertsch, T. Pröll, Fluidized bed reactor design study for pressurized chemical looping combustion of natural gas, *Powder Technol.* 316 (2017) 569–577.
- [15] A. Zaabout, S. Cloete, S.T. Johansen, M. Van, S. Annaland, F. Gallucci, S. Amini, Experimental Demonstration of a Novel Gas Switching Combustion Reactor for Power Production with Integrated CO<sub>2</sub> Capture, *Ind. Eng. Chem. Res.* 52 (2013) 14241–14250.
- [16] S. Noorman, M.V.S. Annaland, H. Kuipers, Packed Bed Reactor Technology for Chemical-Looping Combustion, *Ind. Eng. Chem. Res.* 46 (2007) 4212–4220.
- [17] A. Zaabout, S. Cloete, S. Amini, Autothermal operation of a pressurized Gas Switching Combustion with ilmenite ore, *Int. J. Greenh. Gas Control* 63 (2017) 175–183.
- [18] A. Tong, L. Zeng, M.V. Kathe, D. Sridhar, L.-S. Fan, Application of the Moving-Bed Chemical Looping Process for High Methane Conversion, *Energy & Fuels* 27 (2013) 4119–4128.
- [19] T.-L. Hsieh, D. Xu, Y. Zhang, S. Nadgouda, D. Wang, C. Chung, Y. Pottimurphy, M. Guo, Y.-Y. Chen, M. Xu, P. He, L.-S. Fan, A. Tong, 250 kW<sub>th</sub> high pressure pilot demonstration of the syngas chemical looping system for high purity H<sub>2</sub> production with CO<sub>2</sub> capture, *Appl. Energy* 230 (2018) 1660–1672.

- [20] S.F. Håkonsen, R. Blom, Chemical Looping Combustion in a Rotating Bed Reactor – Finding Optimal Process Conditions for Prototype Reactor, *Environ. Sci. Technol.* 45 (2011) 9619–9626.
- [21] C.O. Iloje, Z. Zhao, A.F. Ghoniem, Design and techno-economic optimization of a rotary chemical looping combustion power plant with CO<sub>2</sub> capture, *Appl. Energy*. 231 (2018) 1179–1190.
- [22] A. Zaabout, S. Cloete, S. Amini, Innovative Internally Circulating Reactor Concept for Chemical Looping-Based CO<sub>2</sub> Capture Processes: Hydrodynamic Investigation, *Chem. Eng. Technol.* 39 (2016) 1413–1424.
- [23] M. Osman, A. Zaabout, S. Cloete, S. Amini, Internally circulating fluidized-bed reactor for syngas production using chemical looping reforming, *Chem. Eng. J.* 377 (2019) 120076.
- [24] M. Osman, A. Zaabout, S. Cloete, S. Amini, Mapping the operating performance of a novel internally circulating fluidized bed reactor applied to chemical looping combustion, *Fuel Process. Technol.* 197 (2020) 106183.
- [25] T. Mattisson, E. Jerndal, C. Linderholm, A. Lyngfelt, Reactivity of a spray-dried NiO/NiAl<sub>2</sub>O<sub>4</sub> oxygen carrier for chemical-looping combustion, *Chem. Eng. Sci.* 66 (2011) 4636–4644.
- [26] C. Linderholm, A. Abad, T. Mattisson, A. Lyngfelt, 160h of chemical-looping combustion in a 10kW reactor system with a NiO-based oxygen carrier, *Int. J. Greenh. Gas Control.* 2 (2008) 520–530.
- [27] A. Thon, M. Kramp, E.-U. Hartge, S. Heinrich, J. Werther, Operational experience with a system of coupled fluidized beds for chemical looping combustion of solid fuels using ilmenite as oxygen carrier, *Appl. Energy*. 118 (2014) 309–317.
- [28] Magnus Rydén Anders Lyngfelt Tobias Mattisson CaMn<sub>0.875</sub>Ti<sub>0.125</sub>O<sub>3</sub> as oxygen carrier for chemical-looping combustion with oxygen uncoupling (CLOU)—Experiments in a continuously operating fluidized-bed reactor system *International Journal of Greenhouse Gas Control* 5 2 2011 356 366 10.1016/j.ijggc.2010.08.004.
- [29] M. Rydén, M. Johansson, A. Lyngfelt, T. Mattisson, NiO supported on Mg–ZrO<sub>2</sub> as oxygen carrier for chemical-looping combustion and chemical-looping reforming, *Energy Environ. Sci.* 2 (2009) 970.
- [30] A. Abad, J. Adánez, F. García-Labiano, L.F. de Diego, P. Gayán, J. Celaya, Mapping of the range of operational conditions for Cu-, Fe-, and Ni-based oxygen carriers in chemical-looping combustion, *Chem. Eng. Sci.* 62 (2007) 533–549.
- [31] A. Lyngfelt, B. Leckner, T. Mattisson, A fluidized-bed combustion process with inherent CO<sub>2</sub> separation; application of chemical-looping combustion, *Chem. Eng. Sci.* 56 (2001) 3101–3113.
- [32] M. Rydén, A. Lyngfelt, T. Mattisson, Chemical-looping combustion and chemical-looping reforming in a circulating fluidized-bed reactor using Ni-based oxygen carriers, *Energy and Fuels.* 22 (2008) 2585–2597.
- [33] A. Abad, T. Mattisson, A. Lyngfelt, M. Ryden, Chemical-looping combustion in a 300W continuously operating reactor system using a manganese-based oxygen carrier, *Fuel.* 85 (2006) 1174–1185.
- [34] M. Arjmand, M. Keller, H. Leion, T. Mattisson, A. Lyngfelt, Oxygen Release and Oxidation Rates of MgAl<sub>2</sub>O<sub>4</sub>-Supported CuO Oxygen Carrier for Chemical-Looping Combustion with Oxygen Uncoupling (CLOU), *Energy Fuels.* 26 (2012) 6528–6539.
- [35] J.W. Butler, J.R. Grace, High-pressure systems and processes for calcium looping, in: *Calcium Chem. Looping Technol. Power Gener. Carbon Dioxide Capture*, Woodhead Publishing, 2015: pp. 377–408.
- [36] J. Li, J.A.M. Kuipers, Effect of pressure on gas–solid flow behavior in dense gas-fluidized beds: a discrete particle simulation study, *Powder Technol.* 127 (2002) 173–184.
- [37] I. Sidorenko, M.J. Rhodes, Pressure Effects on Gas-Solid Fluidized Bed Behavior Pressure Effects on Gas-Solid Fluidized Bed Behavior, *Int. J. Chem. React. Eng.* 1 (2003).
- [38] P.E.G. Gogolek, J.R. Grace, *Fundamental hydrodynamics related to pressurized fluidized bed combustion*, 1995.
- [39] A.W. Weimer, G.J. Quaderer, On dense phase voidage and bubble size in high pressure fluidized beds of fine powders, *AIChE J.* 31 (1985) 1019–1028.
- [40] D.F. King, D. Harrison, Dense phase of a fluidised bed at elevated pressures, *Trans. Inst. Chem. Eng.* 60 (1982) 26–30.
- [41] M. Tsukada, D. Nakanishi, M. Horio, The effect of pressure on the phase transition from bubbling to turbulent fluidization, *Int. J. Multiph. Flow.* 19 (1993) 27–34.
- [42] A. Mahapatro, P. Mahanta, K. Jana, Hydrodynamic study of low-grade Indian coal and sawdust as bed inventory in a pressurized circulating fluidized bed, *Energy.* 189 (2019) 116234.
- [43] Y. Zhang, F. Lei, Y. Xiao, The influence of pressure and temperature on gas-solid hydrodynamics for Geldart B particles in a high-density CFB riser, *Powder Technol.* 327 (2018) 17–28.
- [44] J.G. Yates, Effects of temperature and pressure on gas-solid fluidization, *Chem. Eng. Sci.* 51 (1996) 167–205.
- [45] S. Cloete, A. Zaabout, S. Amini, The Internally Circulating Reactor (ICR) Concept Applied to Pressurized Chemical Looping Processes, *Energy Procedia.* 114 (2017) 446–457.
- [46] J.H. Cloete, M.N. Khan, S. Cloete, S. Amini, Simulation-Based Design and Economic Evaluation of a Novel Internally Circulating Fluidized Bed Reactor for Power Production with Integrated CO<sub>2</sub> Capture, *Processes.* 7 (2019) 723.
- [47] J.R. Grace, Contacting modes and behaviour classification of gas-solid and other two-phase suspensions, *Can. J. Chem. Eng.* 64 (1986) 353–363.
- [48] K.S. Lim, J.X. Zhu, J.R. Grace, Hydrodynamics of gas-solid fluidization, *Int. J. Multiph. Flow.* 2 (1995) 141–193.
- [49] H.T. Bi, J.R. Grace, Effects of pressure and temperature on flow regimes in gas-Solid fluidization systems, *Can. J. Chem. Eng.* 74 (1996) 1025–1027.
- [50] S.C. Gülen, *Gas Turbines for Electric Power Generation*, Cambridge University Press, 2019.